Atomic and Electronic Origins of a Type-*C* Defect on Si(001)

Takehide Miyazaki
Electrotechnical Laboratory, 1-1-4 Umezono, Tsukuba 305-8568, Japan

Tsuyoshi Uda[1] and Kiyoyuki Terakura[2]
[1]*Joint Research Center for Atom Technology (JRCAT)-Angstrom Technology Partnership, 1-1-4 Higashi, Tsukuba 305-0045, Japan*
[2]*JRCAT-National Institute for Advanced Interdisciplinary Research, 1-1-4 Higashi, Tsukuba 305-0045, Japan*
(Received 6 August 1999)

We present an extensive set of *ab initio* calculations for a type-*C* defect on Si(001). Various models belonging to subsurface defects are studied. A substitutional B in the second surface layer is predicted as a possible atomic origin of this defect. However, H and O coupled with second-layer vacancies and a substitutional C are not responsible for a type-*C* defect. We also discuss how the electronic structure of a type-*C* defect contributes to its specific scanning tunneling microscopy images.

PACS numbers: 61.72.Ji, 61.16.Ch, 68.35.Bs, 73.20.At

A current challenge in the study of the Si(001) surface is construction of artificial atomic-scale objects on this surface [1], whose ultimate goal is to establish "nanotechnologies" of semiconductors [2]. The control of *surface defects* is one of crucially important keys to nanotechnologies, since they may affect seriously the stability and functions of those objects.

According to the pioneering work by Hamers and Köhler (HK) [3], typical defects on Si(001) can be classified into three types (type *A*, type *B*, and type *C*). Type-*A* and type-*B* defects have been well studied and are characterized as a single- and double-dimer vacancy, respectively, which belong to a dimer-defect family [4]. However, there is yet *no consensus* about the atomic structure of a type-*C* defect despite the following important features: (i) In scanning tunneling microscopy (STM) images, a type-*C* defect appears to be a protrusion on one half and a vacancy or depression on the other half of a dimer row [3]. The protrusion is observed on the same position in both occupied and unoccupied states. The occupied-state protrusion is weaker compared with the one on the perfect surface. On the other hand, its unoccupied-state counterpart appears to be much stronger than the one on the perfect surface. (ii) Scanning tunneling spectroscopy (STS) at room temperature suggests that the local electronic structures of type-*A* and type-*B* defects have substantial energy gaps, while that of a type-*C* defect has no energy gap [3]. However, Hata *et al.* [5] recently found that there exists a type-*C* defect which has an energy gap below 200 K. (iii) A type-*C* defect acts as a *phase shifter* in a dimer row, at which alternation of dimer buckling changes the phase by π [6]. (iv) It is fragile against external perturbations caused by STM scan. Extraction of Si atoms with an STM tip preferentially occurs near a type-*C* defect, which is then transformed to a type-*B* defect after extraction [7]. Creation of type-*C* defects is also observed during STM scan [8]. (v) It acts as a preferential sticking site in the initial-stage oxidation [9], suggesting that a type-*C* defect is chemically reactive compared with defect-free terraces and type-*A* and type-*B* defects.

As for the structure of a type-*C* defect, HK suggested first a possibility of a pair of half-missing dimers. In the previous paper [10], however, it was demonstrated that this is unlikely to be a proper model, because its optimized structure does not reproduce room-temperature STM images. Instead, a model with a monovacancy in the second surface layer [10] ["C_{int}" [11]; see Figs. 1 and 2(a)] was proposed. With this model, characteristic STM images of a type-*C* defect can be well explained by its calculated local density of states.

Since the model (C_{int}) was proposed, some additional pieces of experimental information have been obtained about the conditions for the appearance and stability of type-*C* defects: (vi) Generation of type-*C* defects depends on the history of sample preparation. They appear on the sample prepared by removal of an oxide layer, but are scarcely observed on the homoepitaxially grown surface [12]. (vii) Their population increases as a function of time and also strongly depends on the vacuum pressure [13]. However, if the background pressure in the chamber is kept to be very low ($<\sim 5 \times 10^{-12}$ Torr) during both surface

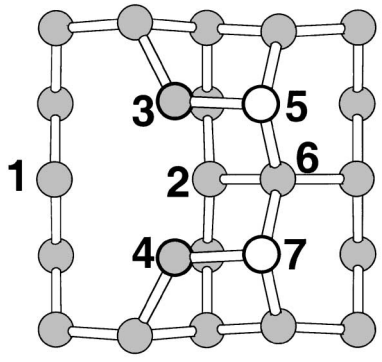

FIG. 1. Basic starting construction of a type-*C* defect [10]. The "up" atoms of dimers are illustrated with open circles. The same convention applies to Fig. 2.

 0031-9007/00/84(18)/4128(4)$15.00

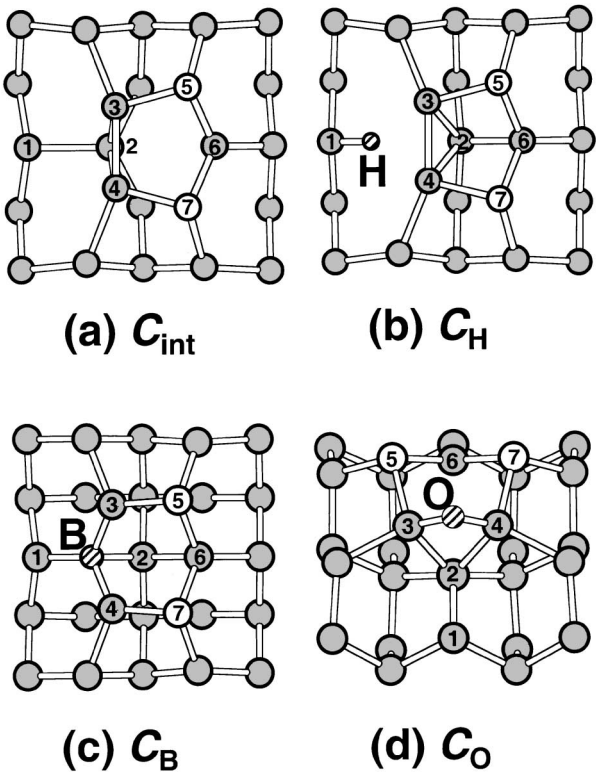

FIG. 2. Optimized structures of (a) C_{int} [10] and its variations with an impurity atom: (b) hydrogen (C_{H}), (c) boron (C_{B}), and (d) oxygen (C_{O}).

preparation and STM observation, then the density of the surface defects is reduced to as low as 1% and a majority of the defects are type *A* [14]. (viii) Type-*C* defects show stiffness during STM scan, in opposition to the fragility mentioned in (iv). Miki observes them even at high temperatures where step flows occur [12].

Judging from these experimental observations, we speculate that there must be other possible type-*C* defects in addition to C_{int} in which some foreign atoms may participate. The impurities may exist (a) in the subsurface and also (b) on top of the surface.

In this Letter, we shed a light on category (a), by extending the previous study for C_{int} [10] to the cases where a type-*C* defect contains an impurity atom. Our viewpoint is supported by the argument by Tersoff that the solubility of any impurity in a crystal may be greatly enhanced near the surface relative to in the bulk [15]. There should be a high possibility with which the type-*C* defects originate from the segregated impurities in the subsurface. Special attention is paid to its chemical reactivity mentioned in (v) and structural stability in (iv) and (viii). We consider as impurities hydrogen (H), carbon (C), boron (B), and oxygen (O) atoms, which are often detected or hard to remove from the surface even in a high vacuum.

We use a standard *ab initio* method based on the density-functional theory [16] in the spin-polarized generalized gradient approximation [17] with plane waves and pseudopotentials. The norm-conserving and the ultrasoft pseudopotentials are used for Si and for H, C, B, and O, respectively [18]. The structures of the type-*C* defect with impurities are simulated with repeated-slab geometries [19].

The optimized structures are illustrated in Fig. 2. The B and C atoms are located in the substitutional positions. We list in Table I the results of structural analysis.

On the perfect Si(001), its highest-occupied and lowest-unoccupied molecular orbital (HOMO and LUMO) states are composed of the dangling-bond (DB) states of the "up" and "down" atoms of each dimer ($|\text{up}\rangle$ and $|\text{down}\rangle$), respectively. If the energy separation between $|\text{up}\rangle$ and $|\text{down}\rangle$ of a certain dimer becomes smaller than the others', then the amplitude of $|\text{up}\rangle$ ($|\text{down}\rangle$) in HOMO (LUMO) decreases (increases) relative to the ground state. Thus, the characteristic STM images of a type-*C* defect mentioned in (i) is reproduced if the constituent dimers (the pairs 3-5 and 4-7) retrieve some character of *symmetric* dimers electronically, but they still preserve a character of buckled dimers geometrically. These two seemingly opposite conditions are satisfied in the C_{int} [10] with a shift of the dimers towards the vacancy and the relaxation of the atom 6 in the second layer. As a result, the θ_{up} increases from 280° to 307°, while the θ_{down} does not change much ($\simeq$356°), reducing the energy separation between $|\text{up}\rangle$ and $|\text{down}\rangle$. Moreover, the change in Δh is small although the z_5 and z_7 [20] decrease due to the relaxation. All vacancy-impurity complex models studied show the similar structural features to C_{int}. These properties essential to the type-*C* defect will not be satisfied when the atomic radii of impurities are greater than that of Si.

In order to compare our results with the observed STM images, we calculate partial probability amplitudes, "$\rho_{\text{occ}}(x, y)$" and "$\rho_{\text{unocc}}(x, y)$" of the states with energies 1.0 eV below and above the Fermi level, respectively [20]. In Fig. 3, we show $\rho_{\text{unocc}}(x, y)$ at 2.0 Å from the surface of the model type-*C* defects except for C_{C}. The bright feature of $\rho_{\text{unocc}}(x, y)$ of the C_{C} does not stand out, and we do not consider C_{C} hereafter.

TABLE I. Summary of the results for a type-*C* defect. Δh, buckling of the constituent dimers, defined as $\Delta h = \frac{(z_5 - z_3) + (z_7 - z_4)}{2}$ [20] (see Fig. 1 for atom indices); θ_{up}, total bond angle of atom 5; $|\beta(\theta_{\text{up}})|^2$, the p_z component of DB on atom 5 [21]; and E_{form}, formation energy of a type-*C* defect. The references of E_{form} are the following: a perfect Si(001) for C_{int}, an H terminating a DB of a dimer ("H_{DB}") for C_{H}, an O inserted in the backbond of a dimer ("O_{BB}") for C_{O}, and a bulk substitutional B ("B_s") and C for C_{B} and C_{C}, respectively [22].

Defect	Δh(Å)	θ_{up}(deg)	$\lvert\beta(\theta_{\text{up}})\rvert^2$	E_{form}(eV)
C_{int}	0.63	301.3	0.46	1.7
C_{H}	0.66	295.0	0.38	3.5
C_{O}	0.75	297.7	0.41	1.9
C_{B}	0.85	291.1	0.33	−0.6
C_{C}	0.91	287.7	0.28	−0.6
Buckled dimer	0.77	277.2	0.12	

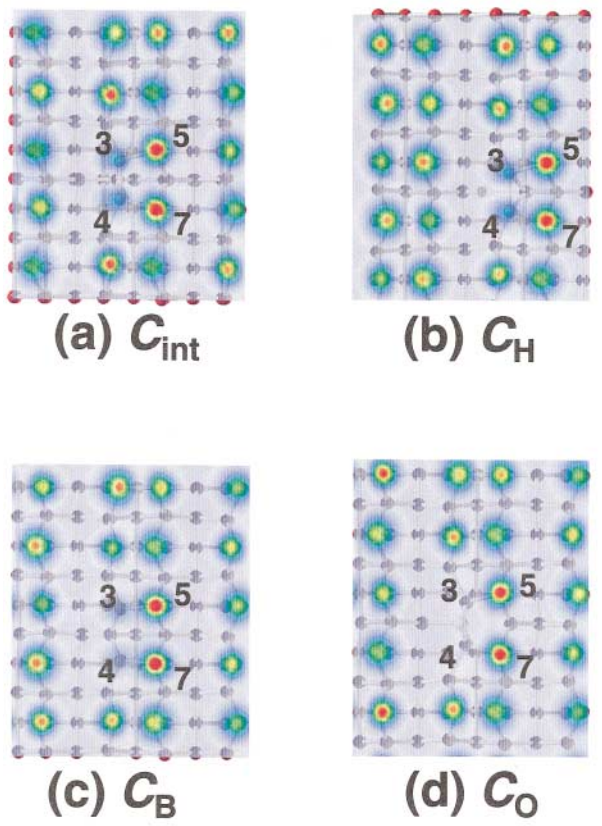

FIG. 3 (color). Spatial distribution of $\rho_{\mathrm{unocc}}(x, y, z_0)$, where z_0 is about 2 Å above the "up" atoms of type-C defects [20]. The spots with larger red regions correspond to larger amplitudes.

We find spin polarization in complex type-C defects, C_B and C_H. There are two roles of spin polarization at a type-C defect: (1) enhancement of the empty-state images and (2) enhancement of chemical reactions with molecules with spins.

First we demonstrate the enhancement of the empty-state images. As discussed above, the electronic properties of a type-C defect may be determined mainly by θ_{up}, and the brightness of empty-state images is expected to line up in the order of C_{int}, C_O, C_H, C_B, and C_C. However, the Fig. 3 shows clearly that the empty-state images of C_O, C_H, and C_B have nearly the similar high intensities to that of C_{int}.

In C_B, an acceptorlike state is produced by the B atom like substitutional B-doping in the bulk, but its energy level emerges in the valence band as a result of the increase in the kinetic energy due to the presence of the surface. The two bonding dimer states (the atom pairs 3-5 and 4-7) split into their bonding and antibonding states through the *inter-dimer* interaction. The former emerges in the valence band, while the latter is pushed up into the gap. The latter originally accommodates two electrons, but, in C_B, one of them occupies the acceptorlike level in the valence band, giving rise to a spin-polarized gap of ~0.1 eV in which the Fermi level is located. Thus the one-fourth of the component of $|\mathrm{up}\rangle$ in HOMO moves to the $|\mathrm{down}\rangle$ counterpart in LUMO, leading to the darker (brighter) filled- (empty-) state images. By the same token, we can exclude the donor-type impurity from the complex type-C defect model, which would produce the brighter (darker) filled- (empty-) state images.

The similar situation arises in C_H. We find that the electronic structure of C_H resembles an acceptor-type defect. The DB on atom 2 in Fig. 2(b) can accommodate one more electron, because the adjacent two atoms (3 and 4) are positively charged. As in the case of C_B, both HOMO and LUMO are originated from the states, having bonding (antibonding) character with respect to intradimer (interdimer) interaction and accordingly the $\rho_{\mathrm{unocc}}(x, y)$ increases. The HOMO-LUMO gap of ~0.2 eV is caused by spin polarization. We show the spin polarization density defined as $\rho^{\uparrow\downarrow}_{\mathrm{occ}}(\mathbf{r}) = \rho^{\uparrow}_{\mathrm{occ}}(\mathbf{r}) - \rho^{\downarrow}_{\mathrm{occ}}(\mathbf{r})$ in Fig. 4, where the positive and negative regions are colored with yellow and blue, respectively. The spin polarization is mainly localized on atoms 5 and 7 with considerable p-characters. The large, yellow parts and thin, blue regions on these atoms are caused by a difference in the positions of lobes and nodal planes of the p orbitals with ↑ and ↓ spins, respectively. Although atom 2 is doubly occupied by the electrons, the distributions of $\rho^{\uparrow}_{\mathrm{occ}}(\mathbf{r})$ and $\rho^{\downarrow}_{\mathrm{occ}}(\mathbf{r})$ differ due to spin polarization, giving rise to the specific distribution of $\rho^{\uparrow\downarrow}_{\mathrm{occ}}(\mathbf{r})$ around this atom.

Because of the spin polarization described above, the bright features in $\rho_{\mathrm{unocc}}(x, y)$ of C_B and C_H stem not only from the antibonding but also from bonding *inter-dimer* states. This is the additional effect to the originally proposed intensity enhancement mechanism of the empty-state image [10]. Since the gaps of C_B and C_H are small, they may look *metallic* in the STS measurements, where large uncertainties are inevitable close to the Fermi level.

Second, and the more significant role of spin polarization at a type-C defect, is enhancement of chemical reactions with molecules with spins, such as O_2. As mentioned in (v) in the introduction, a type-C defect is sensitive to O_2 molecules, which *lose* spin polarization after chemisorption. For this process to occur on the ideal surface which

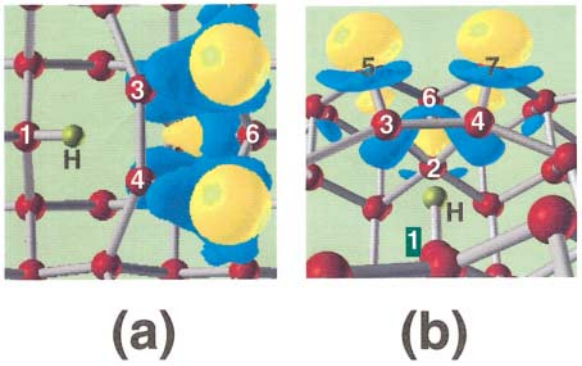

FIG. 4 (color). Spin polarization density (see text) of C_H. (a) A "top" view. (b) A "birds-eye" view.

is spin-nonpolarized, spin conversion via the spin-orbit interaction must be involved, which is very small in oxygens. In fact, Kato *et al.* [23] pointed out that the oxidation of the ideal Si(001) is hampered due to the small spin conversion probability of O_2 molecules. In contrast to this, at the spin-polarized defects on Si(001), the reactions may occur with a greater probability.

Next, we discuss energetics of the type-C defect models. In Table I, we list their formation energies (E_{form}). A positive (negative) value of E_{form} means that the formation of a type-C defect from the specified references (see the caption of Table I for the references) costs (gains) the energy by the amount of $|E_{\text{form}}|$.

Both of the C_{H} and C_{O} are unlikely to be the origins of a type-C defect because of high energy costs for their formation, 3.5 eV [24] and 1.9 eV relative to the references H_{DB} and O_{BB}, respectively (see the caption of Table I for notations of the references).

In sharp contrast, C_{B} is favorable ($E_{\text{form}} = -0.6$ eV) to form relative to B_s [25]. The B atoms are unintentionally introduced into the crystal depending on sample-cleaning procedures [12]. It is reasonable to assume that some of such B atoms are positioned at the antiphase boundaries of dimer rows which are then observed as type-C defects with STM. Although we have little experimental knowledge about how the B atoms are supplied onto the surface [12], the C_{B} is stable undoubtedly. Therefore we propose that C_{B} is a possible origin of type-C defects which are *stiff*.

We find $E_{\text{form}} = 1.7$ eV for C_{int}. Considering the configurational entropies of the vacancy in the second layer and the adatom on the surface, the equilibrium concentration is approximately $\exp(-E_{\text{form}}/2k_{\text{B}}T)$, corresponding to $\sim 10^{-4}$ of one monolayer at $T \sim 1000$ °C, a typical temperature for surface cleaning. This concentration appears too small to explain the existence of *fragile* type-C defects. One should consider another atomic origin: atoms attached on the surface [category (b)]. Representative candidates of such atoms may be H_2O, H, OH, CO, etc. For example, Chander *et al.* [28] propose that a pair of two H_2O molecules adsorbing on two dimers nondissociatively should be responsible for a type-C defect.

In conclusion, our *ab initio* calculations predict that a substitutional boron in the second surface layer (C_{B}) is a possible atomic origin of a type-C defect on Si(001). On the other hand, hydrogen and oxygen atoms in the second-layer vacancies and also a substitutional carbon are unlikely to be atomic origins of this defect. The C_{B} is spin polarized and expected to be sensitive to oxidation. It is structurally stiff and appears metallic at high temperatures. We also present how the electronic structure of a type-C defect is reflected in its characteristic STM images.

This work is partly supported by NEDO.

[1] T.-C. Shen *et al.,* Science **268**, 1590 (1995).
[2] Y. Wada *et al.,* J. Appl. Phys. **74**, 7321 (1993); J. Dabrowski *et al.,* Adv. Solid State Phys. **38**, 565 (1999).
[3] R. J. Hamers and U. K. Köhler, J. Vac. Sci. Technol. A **7**, 2854 (1989).
[4] J. Chang and M. J. Stott, Physica (Amsterdam) **252B**, 127 (1998).
[5] K. Hata *et al.,* Surf. Sci. **447**, 156 (2000).
[6] H. Tochihara *et al.,* Phys. Rev. B **50**, R12 262 (1994); Y. Nakamura *et al., ibid.* **55**, 10 549 (1997).
[7] A. Kobayashi *et al.,* Phys. Rev. B **49**, 8067 (1994).
[8] Z. Zhang *et al.,* Surf. Sci. **369**, L131 (1996).
[9] Ph. Avouris and D. Cahill, Ultramicroscopy **42–44**, 838 (1992); M. Udagawa *et al., ibid.* **42–44**, 946 (1992).
[10] T. Uda and K. Terakura, Phys. Rev. B **53**, 6999 (1996).
[11] The subscript "int" of C_{int} denotes "intrinsic" in the sense that no foreign atoms participate in the model.
[12] K. Miki *et al.,* Surf. Sci. **406**, 312 (1998); (private communication).
[13] K. Hata *et al.,* Surf. Sci. **441**, 140 (1999).
[14] T. Yokoyama and K. Takayanagi, Phys. Rev. B **57**, R4226 (1998); (private communication).
[15] J. Tersoff, Phys. Rev. Lett. **74**, 5080 (1995).
[16] M. C. Payne *et al.,* Rev. Mod. Phys. **64**, 1045 (1992).
[17] J. P. Perdew *et al.,* Phys. Rev. B **46**, 6671 (1992). The use of generalized gradient approximation (GGA) is necessary for accurate calculations of total energies of the models with impurity atoms studied here. The energy gap of C_{int} is 0.50 eV (0.41 eV) with GGA (local density approximation, LDA) by using a 4×5 (4×7) surface supercell. The energy gap of 0.3 eV for C_{int} given in Ref. [10] is obtained including the broadening widths of the delta functions. The difference between the GGA and LDA values ($\sim$0.1 eV) mainly originates from the size difference of the surface cells used. The numerical uncertainty of the energy gap of C_{int} due to different functionals (the Wigner interpolation formula was used in Ref. [10]) is less than 0.05 eV.
[18] N. Troullier and J. L. Martins, Phys. Rev. B **43**, 1993 (1991); K. Laasonen *et al.,* Phys. Rev. B **47**, 10 142 (1993). Cutoff energies of wave functions for C_{int}, C_{H}, C_{B}, C_{O}, and C_{C} defects are 9.0, 12.25, 19.0, 20.25, and 19.0 Ry, respectively.
[19] The supercells have the $p(4 \times n)$ ($n = 5$ or 7) surface periodicity and the 10 or 14 atomic-layer thickness.
[20] Throughout this paper, (x, y) and z denote the surface-parallel and normal coordinates, respectively.
[21] $|\beta(\theta)|^2 = 3[1 - \frac{1}{1-\cos(\theta/3)}]$. See M. C. Desjonquères and D. Spanjaard, in *Concepts in Surface Physics* (Springer, Berlin, 1996), 2nd ed., p. 269.
[22] The reservoir of Si atoms is assumed to be a bulk Si crystal.
[23] K. Kato *et al.,* Phys. Rev. Lett. **80**, 2000 (1998).
[24] For E_{form} of C_{H}, we used the energy gain due to the creation of a H_{DB} from H_2 obtained by E. Pehlke and P. Kratzer [Phys. Rev. B **59**, 2790 (1999)], which is $\sim$2.0 eV.
[25] The same values of E_{form} for C_{B} and C_{C} are mainly because of their similarity in the atomic radii. Our *ab initio* calculated formation energy of C_{C} supports the Tersoff's, ~ -0.7 eV [15]. The C atoms segregated at the subsurface form an alloy with Si which produces the $c(4 \times 4)$ reconstruction [12,26,27].
[26] K. Miki *et al.,* Appl. Phys. Lett. **71**, 3266 (1997).
[27] O. Leifeld *et al.,* Phys. Rev. Lett. **82**, 972 (1999).
[28] M. Chander *et al.,* Phys. Rev. B **48**, 2493 (1993).